Computational Modeling of a High Power Plasma Source for Material Interaction Experiments

IEPC-2013-224

Presented at the 33rd International Electric Propulsion Conference,
The George Washington University • Washington, D.C. • USA
October 6 – 10, 2013

Christopher A. Dodson,[1] Richard E. Wirz[2], and Taylor S. Matlock[3]
University of California, Los Angeles, CA, 90095

Abstract: The UCLA Plasma Interactions facility is being developed to characterize the plasma-material interactions of materials designed for electric propulsion and pulsed power applications. The hybrid fluid/PIC plasma model DC-ION, originally designed to simulate ion thruster discharges, has been modified to simulate this facility. Preliminary results show agreement with the plasma behavior measured in the facility at lower power levels and also reveal important areas where the model can more accurately simulate the facility at full power. This model is being used to optimize the plasma source, complement diagnostics, and provide input for sheath and plasma-material models.

Nomenclature

B	=	magnetic field strength
μ_0	=	permittivity of free space
k	=	Boltzmann's constant
$I_{coil,a}$	=	current through anode coil
I_d	=	discharge current
T_p	=	primary electron temperature
T_e	=	plasma electron temperature
T_o	=	neutral gas temperature
ϕ	=	potential
V_p	=	potential energy of primary electron
V_c	=	potential drop through cathode discharge
V_d	=	discharge voltage
$Q_{in,c}$	=	volumetric flow rate of supply gas through cathode
$Q_{in,a}$	=	volumetric flow rate of supply gas through anode plenum
J_p	=	current of primary electron macroparticle
$J_{p,tot}$	=	total current carried by primary electrons
n_i	=	ion density
n_s	=	plasma electron density
n_o	=	neutral gas density
$\dot{n}_i$	=	ion generation rate density
$\dot{n}_s$	=	plasma electron generation rate density
Γ_i	=	ion flux

[1] Graduate Student, Mechanical and Aerospace Engineering, cdodson17@gmail.com
[2] Assistant Professor, Mechanical and Aerospace Engineering, wirz@ucla.edu
[3] Postdoctoral Researcher, Mechanical and Aerospace Engineering, tmatlock17@ucla.edu

Γ_e = plasma electron flux
$\eta_{ud[gas]}$ = mass utilization efficiency calculated in neutral gas model
$\eta_{ud[beam]}$ = mass utilization efficiency calculated in ion diffusion model

I. Introduction

The major challenge for engineering advanced materials for electric propulsion (EP) applications is determining the material's stability in relevant plasma and high heat-flux environments. Besides the well-known sputtering of the surfaces that can cause erosion of the material and surface morphology changes, preferential sputtering will cause stoichiometry changes that alter the desirable characteristics of the surface with exposure time. In addition, plasma bombardment of the surface creates new issues by providing charge neutralization of semiconductor or insulating surfaces, which can enhance the flux and power density of the charged species, and by ionizing and returning some of the sputtered materials to the surface (redeposition) that further re-engineers the material properties. High heat flux environments can produce complementary changes by preferential evaporation and diffusion of the material components on the surface.

It is critically important to characterize the performance and stability of material surfaces, and especially microarchitectured materials[1], in representative plasma and high heat flux environments. This type of work was pioneered at UCLA 25 years ago[2,3] for the fusion-research community, using hydrogen and deuterium plasma sources for low-Z materials (Be, C) for the walls and high-Z materials (W, Ta) for diverter components. For the current effort we are employing similarly well characterized plasma discharges in gases used in electric propulsion (Xe, Kr, Ar) to bombard the newly microarchitectured materials to characterize their stability and sputtering rates.

Plasma-material interactions primarily manifest in the plasma sheath region where non neutral plasma conditions, high gradients, material sputtering/redeposition, secondary electron emission, high heat flux, and ionization of sputtered material combine to cause a dynamic and poorly understood environment. To help understand this environment, high-resolution, physics-based models that can accept input conditions from the bulk plasma and material surface are being employed in the sheath and pre-sheath regions[4]. In this way, multi-dimensional behavior of the bulk plasma's pre-sheath and sheath in the presence of a featured material surface can be modeled without the typical flat sheath approximation that limits many sheath models[5].

The objective of this effort is to use detailed computational modeling to optimize the facility to deliver high plasma flux to the material surface. Aspects that can be optimized include plasma column diameter and length, plasma density and temperature flatness, neutral gas injection and rate, and plasma density. Due to the wide range of applicability of these "plasma resilient" materials, computational efforts are also being used to interrogate the experimental results and create physics-based material models[6] that can accurately examine material behavior over a wide range of plasma conditions. For example, material life models will be needed to examine long-term performance for thruster applications, since thruster life is typically on the order of 10's of thousands of hours. For pulsed power applications, the computational effort examines high-density, high-energy conditions beyond those that can be reproduced in the laboratory environment.

This paper begins with a brief description of the Plasma-Interactions (Pi) facility, shown in Fig. 1, followed by a description of the DC-ION model and modifications, and presents preliminary results along with future work.

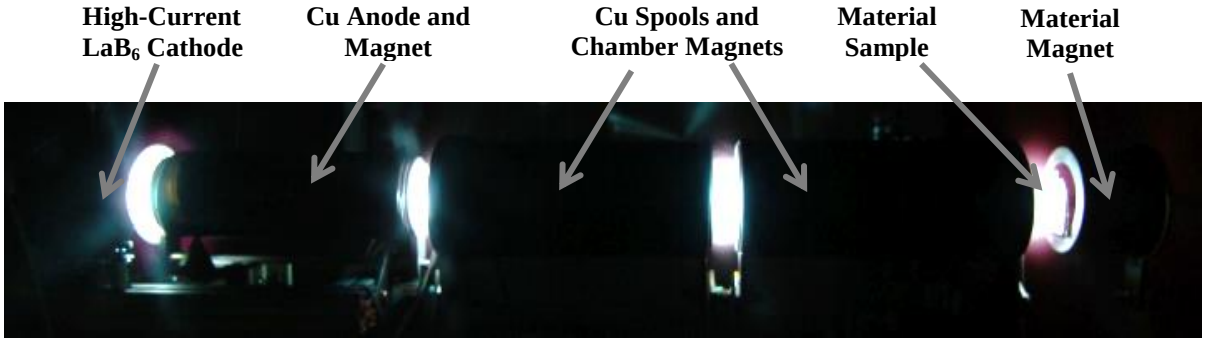

Figure 1. The UCLA Plasma Interactions (Pi) facility during a xenon test (using wide angle lens).

II. Facility Description

The Pi facility consists of a high current LaB_6 hollow cathode that delivers plasma to a series of electromagnets that confine and guide the plasma species to the material surface at end of the plasma column[7]. The source is capable of up to 250 A current steady state and is floating with respect to ground; the chamber magnet spools are grounded. The sample material is biased negatively to repel electrons. The neutral gas propellant, typically xenon or argon, is supplied through the cathode orifice and a plenum near the anode. The addition of the anode gas injection was motivated by research that showed reduced cathode plume oscillations and production of energetic charge-exchange ions that can sputter erode the keeper face and anode[8,9]. It has also been demonstrated to increase the ion current delivered to the target[7]. Diagnostics used to characterize the plasma include Langmuir, double, and emissive probes to provide plasma temperature, density, and potential measurements. In addition to steady-state exposure testing, the facility is being upgraded to allow for high-speed, high-current switching of the target bias to create the conditions relevant to pulsed power applications.

III. Model Description

DC-ION is a 2.5D hybrid/particle-in-cell model developed for DC ion thruster discharges[10,11], depicted in the flow chart in Fig. 2. A hybrid approach was chosen to minimize run times and maximize its effectiveness as a design tool. This multi-species model simulates neutrals, primary electrons, plasma electrons, and ions in the bulk plasma. Primary electrons are treated as individual macroparticles and plasma electrons and ions are treated as fluids. The magnetic field mesh is orthogonal due to the near-uniform magnetic field within the Pi device, although the model possesses the capability of using a magnetically aligned mesh to reduce numerical diffusion and run-time. The neutral gas sub-model assumes free molecular flow due to a Knudsen number (for neutral-neutral and charge exchange collisions) greater than 1. Neutral gas density is then calculated using view factors and depletion due to ionization and charge exchange collisions. Primary electron particle trajectories are calculated using a modified-Boris particle tracking technique[10,11,12]. The ion diffusion sub-model calculates ion diffusion and accounts for non-classical cross-field diffusion using effective mobilities based on the relative rate of electron-ion collisions compared electron-neutral collisions. In the electron thermal sub-model, plasma electron temperature is determined by using effective potentials to determine electron flux, then solves the electron energy equation for plasma electrons.

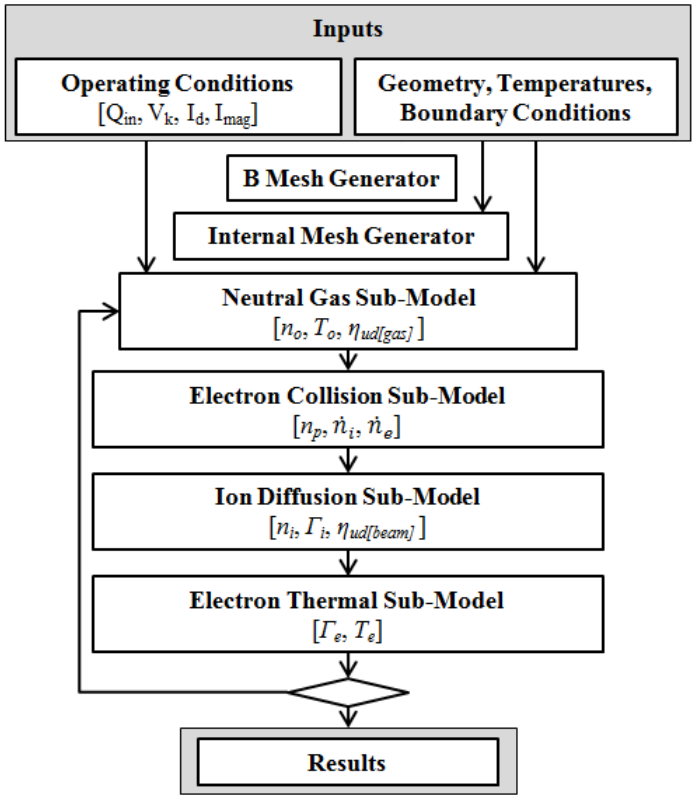

Figure 2. Multi species hybrid fluid-PIC model flow chart.

IV. Model Modifications

This section will describe the modifications to DC-ION for modeling the Pi facility. The fundamental assumptions have not changed from their original formulation, but there have been several changes to the geometry of the simulation domain, boundary conditions, and the neutral gas and primary electron sub-models.

A. Internal and Boundary Meshes

The overall geometry of the model is depicted in Fig. 3, including the current and neutral gas injection locations (at the cathode orifice and an annular plenum located between the keeper face and anode). Each is considered to emit neutrals in the directions shown with a cosine velocity distribution. The internal and boundary meshes are shown in Fig. 4. An orthogonal internal mesh was chosen due to being nearly aligned with the magnetic field lines, although future upgrades will include using a magnetic field aligned mesh to improve accuracy. Only the area within the coils is considered in the simulation domain. The boundary mesh consists of cathode face, anode, chamber magnet, target, and gap surface types for assessing the various energy losses within the system and specifying boundary conditions such as temperature and electric potential. For example, electrons are considered repelled from both the cathode face and target, but can be lost to the anode, chamber magnet spools, and through the gaps. Ions can be lost to the anode, target, and gaps, but losses to the cathode are ignored.

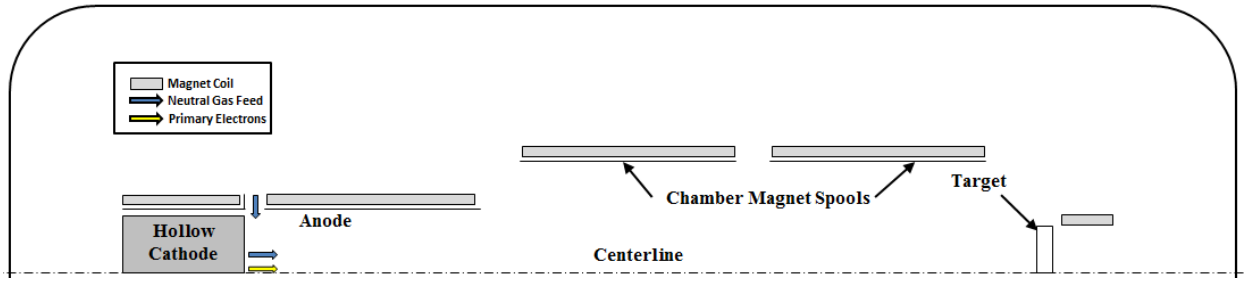

Figure 3. Geometry of the Pi configuration used in DC-ION (not to scale).

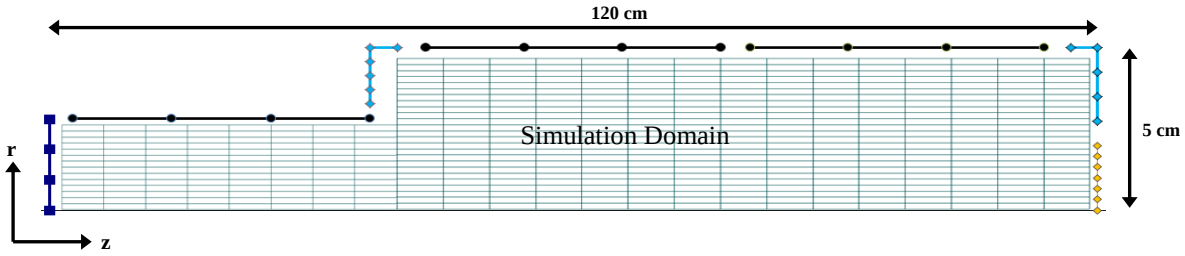

Figure 4. Internal and surrounding boundary mesh.

B. Neutral Gas Model

The gas model from DC-ION is based on a view factor based approach that can simulate a variety of gas sources, device geometries, wall temperatures, and surface transparencies. This model was slightly modified to also include the effects of the vacuum facility background gases on the gas properties within the simulation domain. Neutral gas incident on a boundary are considered re-emitted in a cosine distribution with at a temperature corresponding to the wall temperature. The background neutral gas flux at the gaps of the Pi device are treated as sources at the gap boundaries with a temperature equal to that of the vacuum chamber wall. This flux is $n_{o,BG}\bar{v}_{o,BG}/4$, where $\bar{v}_{o,BG}$ is the average thermal velocity, $\sqrt{(8kT_{o,BG})/(\pi m_o)}$, $T_{o,BG,}$ is the background gas temperature, and $n_{o,BG}$, is the background gas density determined from chamber pressure measurements.

C. Magnetic Field Mesh Generation

In the particle tracking algorithm for simulations of ion thrusters using DC-ION, the magnetic field at the primary electron location was calculated at each time step because it was critical to have accurate values of magnetic fields near the cusps. For Pi, to improve run time the magnetic field mesh is generated using analytical expressions for the magnetic field of a current loop[13], summing the contributions of each loop for each node location, as shown in Equations 1 and 2.

$$B_z = \frac{\mu_0 I}{2\pi\sqrt{(r+r_l)^2+(z-z_l)^2}}\left[K(m)+\left(\frac{2r_l(r+r_l)}{[(r+r_l)^2+(z-z_l)^2\,](1-m)}-\frac{1}{1-m}\right)E(m)\right] \quad (1)$$

$$B_r = \frac{\mu_0 I(z-z_l)}{2\pi\sqrt{(r+r_l)^2+(z-z_l)^2}}\left[\frac{K(m)}{r}-\frac{E(m)}{r(1-m)}+\frac{2aE(m)}{[(r+r_l)^2+(z-z_l)^2\,](1-m)}\right] \quad (2)$$

where r is the radial location of the node, r_l is the loop radius, I is the current through the loop, z is the axial location of the node, z_l is the axial location of the loop, $K(m)$ and $E(m)$ are complete elliptic integrals of the first and second kind, respectively, and m is the square of the elliptic modulus given by $4rr_l/[(r+r_l)^2+(z-z_l)^2]$. Figure 5 shows a contour plot of the magnetic field throughout the simulation domain, with magnetic field lines (originating from the cathode orifice) illustrating the curvature near the gaps and convergence near the target.

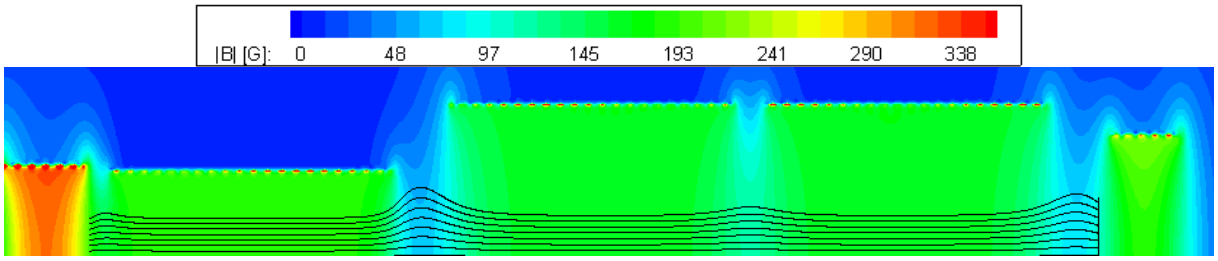

Figure 5. Magnetic field magnitude.

D. Primary Electron Model

The primary electron model inputs are the electron temperature and energy. The relevant potentials in the discharge are depicted in Figure 6, along with a representative plasma potential profile based on measurements by Matlock et al[14]. Measurements taken by emissive probes at both the anode and target cross-sections have shown a hollow potential profile. Primary electrons are emitted from the cathode insert at cathode potential and lose approximately 5 eV (denoted as V_c in the figure) due to resistivity in within the cathode. The electrons exit the cathode with an estimated thermal energy of 2-3 eV and are accelerated into the discharge by the bulk plasma potential. Since the electrons are predominantly confined to the centerline we use V_p (a constant) as an estimate for the accelerating potential for each primary electron.

For ion thruster simulations, due to the small size of the cathode orifice it can be assumed that the primary electrons are emitted as a point source. Since the Pi hollow cathode orifice is approximately 1 cm in diameter, a uniform distribution of primaries is assumed instead. Each primary macro-particle represents the same amount of discharge current with the initial radial location determined by area weighting of the orifice face (Eq. 3).

$$r_i = \left(\frac{i\,{r_{co}}^2}{N}\right)^{1/2} \quad (3)$$

where r_i is the initial radial location, i is the macro-particle number, r_{co} is the cathode orifice radius, and N is the total number of particles used to represent the total cathode electron current.

The particle tracking algorithm determines the position of the primary electron particles using a modified Boris predictor-corrector scheme[10,11,12]. The trajectory is affected by both electric and magnetic fields, but as a first approximation we neglect the electric field due to the assumption of constant plasma potential near the centerline. The magnetic field input into the particle tracking algorithm is obtained through bilinear interpolation (area weighting) of the magnetic field mesh in the r-z plane as shown in Eq. 4.

$$B_{iP} = \frac{(B_{i1}r_2 + B_{i2}r_1)z_2 + (B_{i3}r_2 + B_{i4}r_1)z_1}{(r_1 - r_2)(z_1 + z_2)} \quad (4)$$

where P is the particle location, i represents the r- or z-component, $B_{i1\text{-}4}$ are the magnetic field values at the nearest nodes, and $r_{1\text{-}4}$ and $z_{1\text{-}4}$ represent the distances to the nearest nodes.

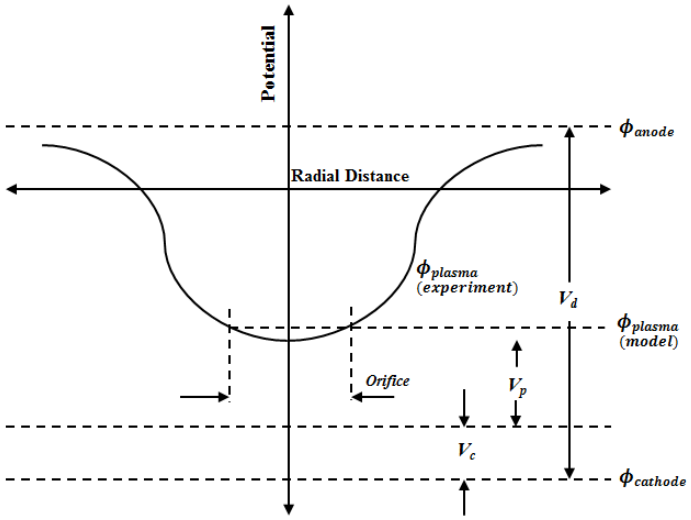

Figure 6. Potentials relevant to primary electrons.

The trajectory of a single particle emitted from near the cathode orifice edge is shown in Fig. 7, demonstrating that the particle follows the magnetic field lines and is reflected at the target. Due to the confining magnetic field, nearly all primary electron particles are ultimately depleted due to the collective inelastic collisions with plasma species, shown in the figure. Typically at least 20 macroparticles are used to represent the total emitted current.

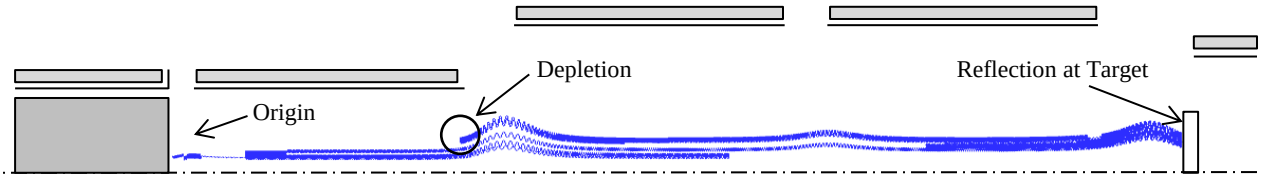

Figure 7. Primary electron trajectory.

V. Results

Preliminary results were obtained for low-power operating conditions as listed in Table 1. As shown in Fig. 8, the primary electrons are confined near the centerline by the strong axial magnetic field. Figure 9 shows a high neutral gas density in the anode region compared to the downstream region. High primary electron and neutral gas densities result in a short mean free path, and therefore high ionization rates and ion densities as shown in Figs. 10 and 11. Downstream of the anode ionization rate and ion density correspond with regions of high primary electron density, which is reasonable since primary electrons are the predominant energy source. Figure 12, an image of the plasma column between the chamber magnets, visually confirms the high concentration of plasma near the centerline. Higher-power operating conditions proved difficult to obtain convergence and so future efforts will explore those regimes as well.

Table 1. Low-Current Operating Conditions

Propellant	Power (W)	V_d (V)	I_d (A)	$I_{coil,a}$ (A)	V_p (V)	$Q_{in,a}$ (sccm)	$Q_{in,c}$ (sccm)	T_p (eV)	ϕ_{plasma} (V)	$P_{background}$ (Torr)
Xenon	150	34	15	22	10	10	10	2.5	-15	4e-6

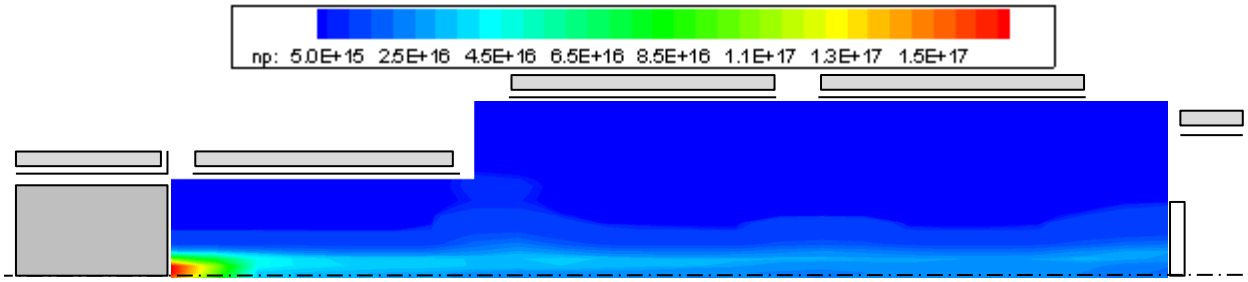

Figure 8. Primary electron density, m^{-3}.

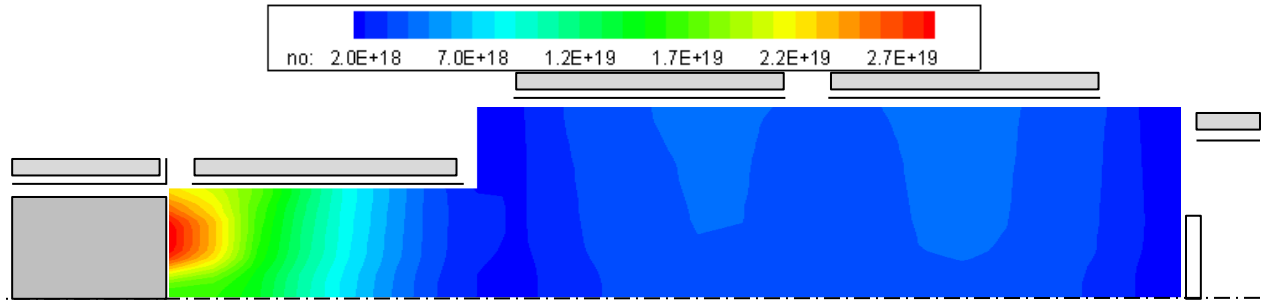

Figure 9. Neutral gas density, m^{-3}.

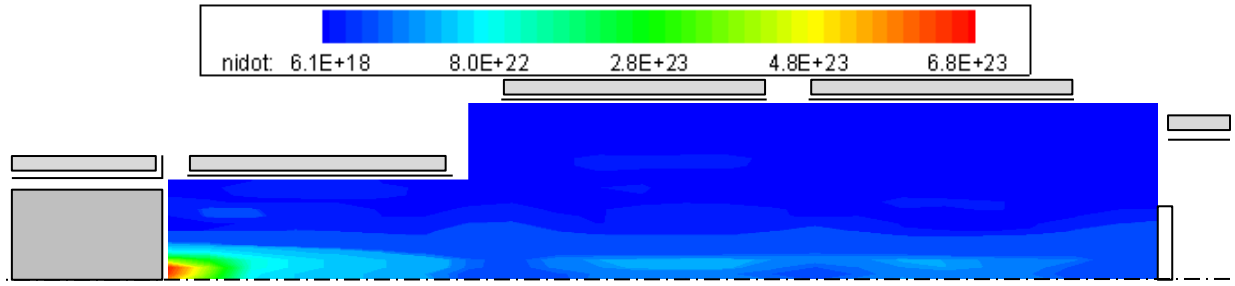

Figure 10. Ionization rate density, s^{-1}-m^{-3}.

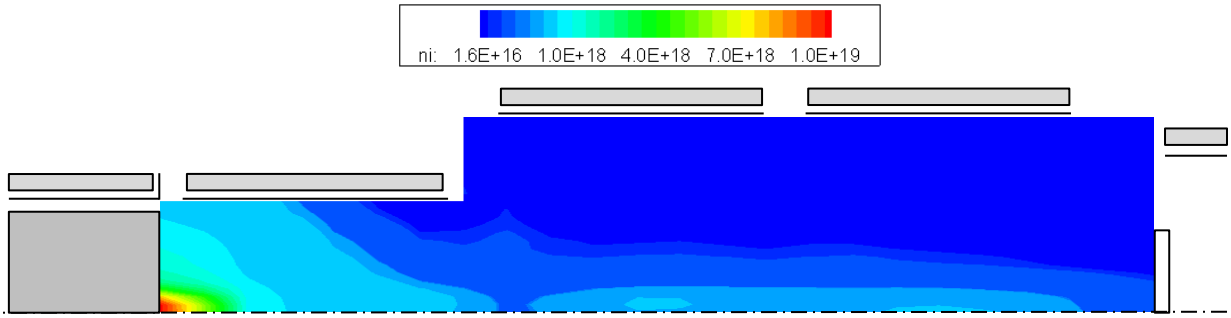

Figure 11. Ion density, m^{-3}.

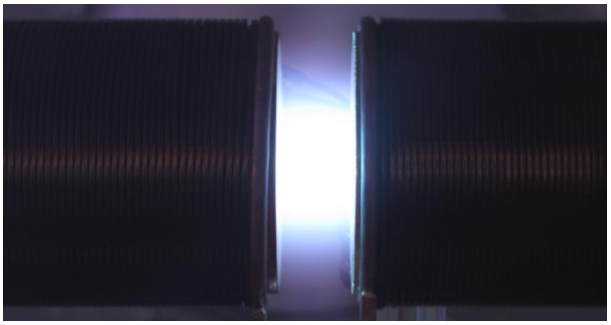

Figure 12. Plasma column between chamber magnets.

For model validation, measurements of plasma density and temperature were taken near the anode exit plane using Langmuir and double probes. An emissive probe was used for measuring plasma potential, which was used to estimate V_p as discussed in IV-D. Figure 13a shows profiles of density for singly charged species as a function of radial distance in the near anode region. These results indicate the presence of a high primary electron content for radii less than 1 cm. The implications of this on the fundamental assumptions of the DC-ION model are being investigated. Plasma temperature results are shown in Fig. 13b and, although low, also show reasonable values of 1.5-2 eV. The simulation results are based on 10 sccm flow through both the cathode and anode plenum, but the experimental results were obtained at 6 sccm through each. A higher massflow was chosen for the simulation due to difficulties converging at the 6 sccm flow rate condition. This was offset by the use of a lower background pressure in the simulation (6e-6 Torr) compared to the experimentally measured value (6e-5 Torr), which will result in an increase in the overall neutral gas density.

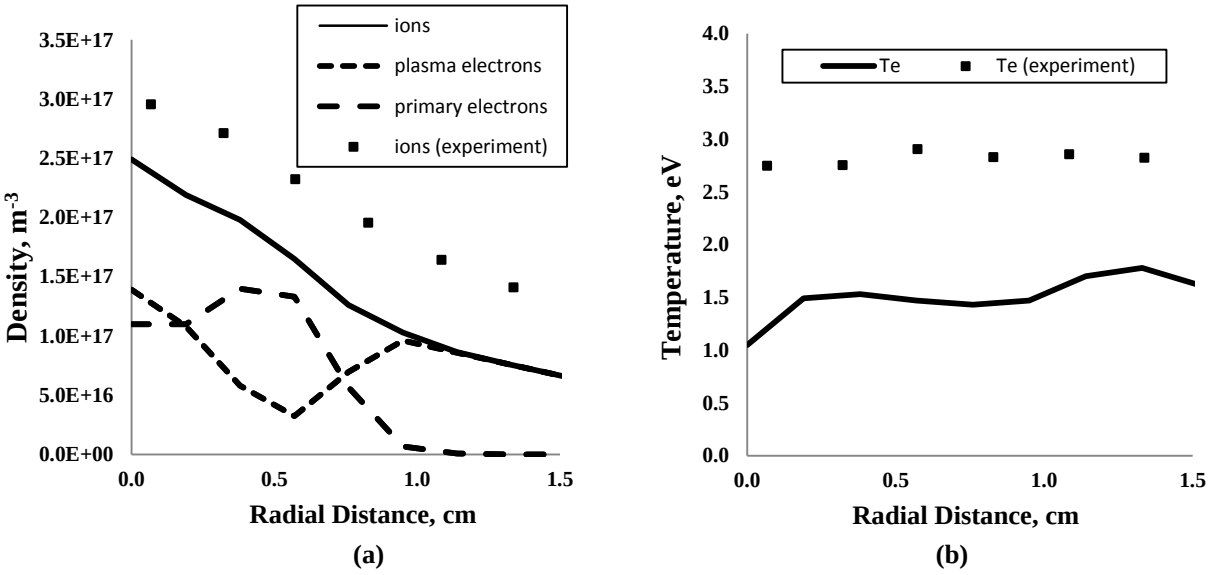

Figure 13. (a) Plasma density profiles and (b) plasma electron temperature near the anode exit plane.

VI. Conclusions and Future Work

The hybrid fluid/PIC model DC-ION has been modified to simulate the Pi facility. Predictions of plasma properties at low-current operating conditions have been obtained and compared to experimental data and agree qualitatively. The results have revealed areas to improve the model for higher current operating conditions. These improvements include utilizing a magnetic field aligned mesh and integrating plasma potential calculations into the primary electron sub-model to improve accuracy of primary electron energy and ionization rates. With improved model accuracy, optimization of the device can be performed for parameters such as column length, target location, and plasma density profile. This model will then be integrated with plasma sheath and material models to enable multi-scale simulations of plasma-material interactions.

Acknowledgments

The author would like to thank Samuel Araki for support on the computational model development. This work is funded by the U.S. Air Force Office of Scientific Research under grants FA9550-11-1-0282 and FA9550-11-1-0029 and the UCLA School of Engineering and Applied Sciences.

References

[1]Sharafat S., Aoyama A., Williams B, Ghoniem N., "Development of micro-engineered textured tungsten surfaces for high heat flux applications," *Journal of Nuclear Materials*, Vol. 442, pp. S302–S308, 2013.

[2]Goebel, D., Campbell, G., Conn, R., "Plasma Surface Interaction Facility-PISCES", *Journal of Nuclear Materials*, Vol. 121, May 1984, pp. 277-282.

[3]Goebel, D., Hirooka, Y., Conn, R., et al., "Erosion and Redeposition Experiments in the PISCES Facility," *Journal of Nuclear Materials*, Vols. 145-147, Feb. 1987, pp. 61-70.

[4]Wirz R., Anderson J., Katz I., "Time-Dependent Erosion of Ion Optics," *AIAA Journal of Propulsion and Power*, Vol. 27, No. 1, Jan.-Feb. 2011, pp. 211-217.

[5]Roy S., Pandey, B., Poggie, J., Gaitonde, D., "Modeling low pressure collisional plasma sheath with space-charge effect," *Physics of Plasmas*, Vol. 10, No. 6, June 2003, pp. 2578-2585.

[6]Crosby, T., Ghoniem, N., "Multiphysics model of thermomechanical and helium-induced damage of tungsten during plasma heat transients", *Journal of Nuclear Materials*, Vol. 442, pp. S261–S266, 2013.

[7]Matlock, T., Goebel, D., Conversano, R., and Wirz, R., "The Plasma Interactions Facility at UCLA", *49th Joint Propulsion Conference and Exhibit*, 2013, JPC-2013-4132.

[8]Chu, E., Goebel, D., Wirz, R., "Reduction of energetic ion production in hollow cathodes by external gas injection", *Journal of Propulsion and Power*, Vol. 29, No. 5, Sept.-Oct. 2013, pp. 1155-1163.

[9]Goebel, D., Jameson, K., Katz, I., Mikellides, I., "Potential fluctuations and energetic ion production in hollow cathode discharges", *Physics of Plasmas*, Vol. 14, No. 10, Oct. 2007, pp. 103508-1 to 103508-15.

[10]Wirz, R., "Discharge Plasma Processes of Ring-Cusp Ion Thrusters," Ph.D. Dissertation, Aeronautics, California Institute of Technology, Pasadena, CA, 2005, http://thesis.library.caltech.edu/1974/1/Wirz_Thesis.pdf.

[11]Wirz R., Katz I., "2-D Discharge Chamber Model for Ion Thrusters," *40th AIAA/ASME/SAE/ASEE Joint Propulsion Conference and Exhibit*, Ft. Lauderdale, FL, July 2004, AIAA-2004-4115.

[12] Mao, H.-S. and Wirz, R., "Comparison of Charged Particle Tracking Methods for Non-Uniform Magnetic Fields," *42nd AIAA Plasmadynamics and Lasers Conference*, Honolulu, Hawaii, June 2011, AIAA 2011-3739.

[13]Kuns, K., "Calculation of Magnetic Field Inside Plasma Chamber," Tech. rep., UCLA, 2007.

[14]Matlock, T., Goebel, D., Conversano, R., Wirz, R., "Near anode plasma in the plasma interaction facility at UCLA", *33rd International Electric Propulsion Conference*, Washington, D.C., Oct. 2013, IEPC-2013-327.